ACS APPLIED MATERIALS & INTERFACES

Research Article

www.acsami.org

Efficiency Enhancement of Inverted Structure Perovskite Solar Cells via Oleamide Doping of PCBM Electron Transport Layer

Fei Xia,[†] Qiliang Wu,[†] Pengcheng Zhou,[†] Yi Li,[‡] Xiang Chen,[†] Qing Liu,[†] Jun Zhu,[‡] Songyuan Dai,[‡,§] Yalin Lu,[†] and Shangfeng Yang*[,†]

[†]Hefei National Laboratory for Physical Sciences at Microscale, Key Laboratory of Materials for Energy Conversion, Chinese Academy of Sciences, Department of Materials Science and Engineering, Synergetic Innovation Center of Quantum Information & Quantum Physics, University of Science and Technology of China (USTC), Hefei 230026, China

[‡]Key Laboratory of Novel Thin Film Solar Cells, Hefei Institutes of Physical Science, Chinese Academy of Sciences, Hefei 230031, China

[§]Beijing Key Lab of Novel Thin Film Solar Cells, North China Electric Power University, Beijing 102206, China

Supporting Information

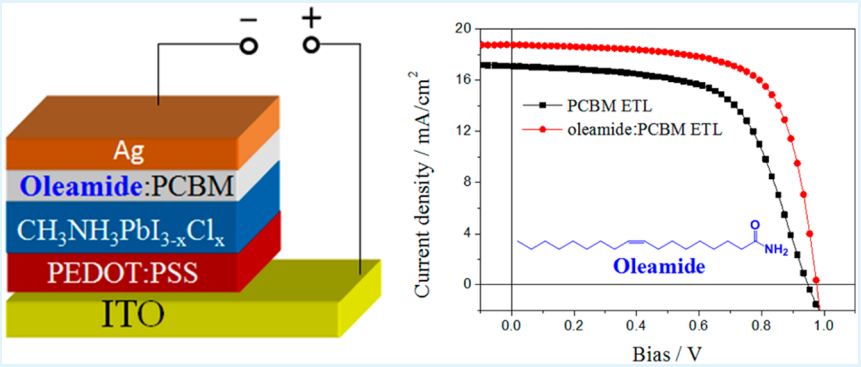

ABSTRACT: An amphiphilic surfactant, oleamide, was applied to dope the PCBM electron transport layer (ETL) of inverted structure perovskite solar cells (ISPSCs), resulting in a dramatic efficiency enhancement. Under the optimized oleamide doping ratio of 5.0 wt %, the power conversion efficiency of the $CH_3NH_3PbI_xCl_{3-x}$ perovskite-based ISPSC device is enhanced from 10.05% to 12.69%, and this is primarily due to the increases of both fill factor and short-circuit current. According to the surface morphology study of the perovskite/PCBM bilayer film, oleamide doping improves the coverage of PCBM ETL onto the perovskite layer, and this is beneficial for the interfacial contact between the perovskite layer and the Ag cathode and consequently the electron transport from perovskite to the Ag cathode. Such an improved electron transport induced by oleamide doping is further evidenced by the impedance spectroscopic study, revealing the prohibited electron−hole recombination at the interface between the perovskite layer and the Ag cathode.

KEYWORDS: *perovskite solar cells, electron transport layer, interface, oleamide, PCBM*

INTRODUCTION

Since the first report of perovskite-sensitized solar cells by Miyasaka et al. in 2009,[1] hybrid organic/inorganic organometal halide perovskite solar cells have been attracting a great deal of attention due to their ever-increasing power conversion efficiencies (PCEs) already exceeding 20%.[2−13] Perovskite solar cells show the advantages of simple fabrication, large absorption coefficients, tunable bandgaps, high carrier mobility, and especially long charge carrier diffusion lengths.[3−5] So far, the most popular and efficient architecture for perovskite solar cells is composed of a light absorber layer, which is mainly an organometal halide such as $CH_3NH_3PbX_3$ (X = I, Br, Cl) sandwiched between a transparent electrode and a metal electrode.[2−13] In addition to the optimization of the composition and the crystallization process and morphology of the perovskite light absorber layer determining the charge carrier generation, the interfaces between perovskite and electrodes play an important role in efficient charge transport and extraction. Thus, interfacial layers including hole transport layers (HTLs) and electron transport layers (ETLs) are usually introduced between the perovskite layer and electrodes so as to improve the perovskite/electrode interfaces, and consequently the performance of perovskite solar cells.[2,6−15] According to the locations of the HTL and ETL relative to the transparent electrode through which the light illuminates, so far two major types of perovskite solar cell structures have been developed,

Received: April 23, 2015
Accepted: June 8, 2015
Published: June 8, 2015

DOI: 10.1021/acsami.5b03525
ACS Appl. Mater. Interfaces 2015, 7, 13659−13665

including a conventional structure, in which ETL clings to the bottom transparent electrode, while the perovskite layer is coated onto the ETL, and an inverted structure where the locations of ETL and HTL are inverted (i.e., HTL contacts with the bottom transparent electrode).[9−16] Although the highest PCE of perovskite solar cells (20.3%) reported until now was obtained for the conventional structure,[10] the inverted structure perovskite solar cells also appear promising for potential commercialization based on the uniqueness of the low-temperature solution processable fabrication, the possibility of low-cost, the large-scale manufacturing, and the high flexibility.[16−25]

For the state-of-the-art solution-processable inverted structure perovskite solar cells (ISPSCs), whose device structure is analogous to that of polymer solar cells,[26] poly(3,4-ethylene dioxythiophene):poly(styrenesulfonate) (PEDOT:PSS) is generally used as an HTL where fullerene derivatives such as [6,6] phenyl-C61-butyric acid methyl ester (PCBM) often act as ETLs.[16−25] Since ETL determines the electron transport from the perovskite layer to the metal cathode, it is highly desirable to improve the uniformity of the PCBM ETL film so as to prohibit the film defects and, consequently, the electron−hole recombination at the perovskite/cathode interface. Thus, much effort has been made to optimize the spin-coating speeds and solvents in order to improve the morphology of the PCBM ETL film.[19−21] Besides, an ultrathin layer, such as Ca,[27] LiF,[28] TiO_x,[16] and amino-functionalized polymer,[29] has also been incorporated between the PCBM layer and the metal cathode via thermal evaporation[18] or spin-coating of alcohol solution,[29−31] so as to modify the metal cathode toward improved electron transport. However, the thermally evaporated ultrathin layer of Ca or LiF may suffer from instability, and alcohol solvent (such as methanol) treatment may suffer from inadequate repeatability of the device performance due to the possible damage of alcohol to the perovskite layer.[29−32] An alternative strategy to improve the uniformity of the PCBM ETL film is to dope the PCBM layer with other compounds, and in this way, introduction of an additional interfacial layer can be avoided. Recently, Zhao, Yang, and Yan et al. added polystyrene (PS) into the PCBM layer and achieved a PCE enhancement from 9.56% to 10.68% due to the better ETL coverage on the perovskite film, resulting in a lower charge carrier recombination rate and longer electron lifetime.[33] Nevertheless, to our knowledge, so far the reports on doping the PCBM ETL of ISPSCs are quite limited. Therefore, it is intriguing to address whether doping the PCBM with small organic molecules would improve the performance of ISPSCs or not.

In this paper, we report the first application of an amphiphilic surfactant, oleamide, in doping the PCBM ETL, resulting in a dramatic efficiency enhancement of the $CH_3NH_3PbI_xCl_{3-x}$ perovskite-based ISPSC devices. The oleamide doping ratio is optimized, and its effects on light absorption and the surface morphology of perovskite/PCBM films as well as the perovskite/cathode interface were investigated, revealing a mechanism for efficiency enhancement upon oleamide doping.

EXPERIMENTAL SECTION

Materials. The indium tin oxide (ITO) glass substrate with a sheet resistance of 10 Ω/sq was purchased from Shenzhen Nan Bo Group, China. PEDOT:PSS (Clevios P Al4083) was obtained from SCM Industrial Chemical Co., Ltd. The material CH_3NH_3I was synthesized in our lab following the procedure reported in ref 34. $PbCl_2$, dimethyl sulfoxide (DMSO), γ-butyrolactone (GBL), and chlorobenzene were purchased from Alfa Aesar. The PCBM was bought from Nichem Fine Technology Co., Ltd. The oleamide ($C_{18}H_{35}NO$, 99%) was purchased from Aldrich. All materials were used as received without further purification.

Device Fabrication. The ITO-coated glass substrates were ultrasonicated in detergent, deionized water, acetone, and isopropanol for 15 min every time, and subsequently dried in an oven overnight. They were cleaned in a UV ozone oven for 12 min prior to use. PEDOT:PSS aqueous solution was first filtered by a 0.45 μm polyvinyl difluoride syringe filter, and then a thin layer (ca. 40 nm thick) of PEDOT:PSS was spin-coated onto the ITO substrates at 3000 rpm for 1 min. They were baked on a hot plate at 140 °C for 10 min in air, and were then transferred into a glovebox filled with dried nitrogen ($O_2 \leq$ 0.1 ppm; $H_2O \leq$ 0.1 ppm). A perovskite photoactive layer was deposited onto the PEDOT:PSS layer by spin-coating a $PbCl_2$/CH_3NH_3I (1:3) blend solution containing 0.8 M (222 mg) $PbCl_2$ and 2.4 M (381 mg) CH_3NH_3I in 1 mL mixed solvents of DMSO:GBL (3:7 v/v) at 5000 rpm for 30 s. Both the perovskite precursor solution and the substrates were preheated at 60 °C for 5 min before spin-coating. After spin-coating the perovskite layer, 50 μL of anhydrous chlorobenzene was quickly injected onto the film and kept for 10 s, followed by spin-coating at 5000 rpm for 30 s again. The yellowish as-cast film was quickly transferred to a hot plate to keep the temperature at 60 °C for 5 min and was then annealed at 100 °C for 20 min. PCBM (20 mg/mL) was first dissolved in anhydrous chlorobenzene, and oleamide was added into the PCBM solution in a variable ratio (1%, 5%, 10%, wt %). A thin layer of oleamide:PCBM was spin-coated onto the cooled perovskite layer at 1500 rpm for 30 s. Finally, the device was transferred into a vacuum chamber (~10^{-5} Torr), and an Ag electrode (ca. 80 nm thick) was thermally deposited through a shadow mask to define the effective active area of the devices (2 × 7 mm^2). The complete devices were transferred back into the glovebox and encapsulated with UV-curable epoxy glue and cover glass slides before testing in air.

Measurements and Characterization. The current density−voltage (J−V) characterization of the ISPSCs was carried out using a Keithley 2400 source measurement unit under simulated AM 1.5 irradiation (100 mW cm^{-2}) with a standard xenon-lamp-based solar simulator (Oriel Sol 3A, U.S.A.). The J−V measurement was carried out under reverse scan with a scan rate of 0.1 V/s. At the same time, a measurement under forward scan was also performed for the best devices to check the hysteresis of the J−V curve. The solar simulator illumination intensity was calibrated by a monocrystalline silicon reference cell (Oriel P/N 91150 V, with KG-5 visible color filter) calibrated by the National Renewable Energy Laboratory (NREL). All of the measurements were carried out in air, and a mask with a well-defined area size of 14.0 mm^2 was attached onto the cell to define the effective area in order to ensure accurate measurement. Dozens of devices were fabricated and measured independently to obtain the statistical histograms of PCE, J_{sc}, and FF of the ISPSCs. The best and average data were used in the following discussions. External quantum efficiency (EQE) was carried out with an ORIEL Intelligent Quantum Efficiency (IQE) 200 Measurement system established with the tunable light source.

The thickness of the film was measured by a KLA-Tencor P6 surface profilometer. X-ray diffraction (XRD) data were measured by a Rigaku SmartLab X-ray Diffractometer. UV−vis spectroscopy was recorded on a UV−vis−NIR 3600 spectrometer (Shimadzu, Japan). The SEM image was obtained on a JSM-7401F instrument (JEOL, Japan). Atomic force microscopy (AFM) measurements were carried out on a Veeco DI-MultiMode V scanning probe microscope in tapping mode using a tip with a sensitivity of 0.1 nm. Impedance spectroscopic measurements were taken using an electrochemical analyzer (Autolab 320, Metrohm, Switzerland) with a variable reverse potential from 0.2 to 0.8 V in the dark. AC 20 mV perturbation was applied with a frequency from 1 MHz to 1 Hz. The obtained impedance spectra were fitted with ZView software (v2.8b, Scribner Associates, U.S.A.). The Nyquist plots and the best fit results are based

DOI: 10.1021/acsami.5b03525
ACS Appl. Mater. Interfaces 2015, 7, 13659−13665

on an equivalent circuit shown in Supporting Information (SI) Figure S4.

RESULTS AND DISCUSSION

Given that the device structure of ISPSC is analogous to that of polymer solar cells, those materials applied as effective ETLs of polymer solar cells[26,35−42] are preferably considered. In particular, oleamide, as an amphiphilic surfactant, was successfully incorporated as the ETL into the poly(3-hexylthiophene-2,5-diyl) (P3HT):PCBM bulk heterojunction polymer solar cells by doping in the P3HT:PCBM photoactive layer, followed by self-assembly, leading to a dramatic enhancement of the device efficiency by ∼28%, which was interpreted by the formation of the interfacial dipole layer facilitating the electron extraction by Al cathode.[42] Motivated by the effectiveness of oleamide as the ETL of bulk heterojunction polymer solar cells with excellent interfacial properties, in our present study we chose oleamide to dope the PCBM ETL of ISPSC.

Oleamide was added into a PCBM solution in a variable ratio (1 wt %, 5 wt %, 10 wt %), and the performance of the corresponding ITO/PEDOT:PSS/$CH_3NH_3PbI_xCl_{3-x}$ perovskite/oleamide:PCBM/Ag ISPSC devices (Figure 1A) were

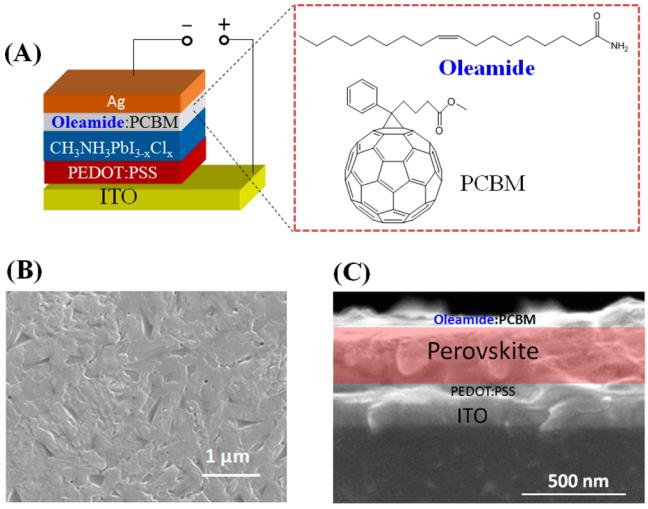

Figure 1. (A) Schematic structure of the ISPSC device and the chemical structures of oleamide and PCBM; (B) surface topographic SEM image of the $CH_3NH_3PbI_xCl_{3-x}$ perovskite film on ITO/PEDOT:PSS substrate; and (C) cross-sectional SEM image of the device without Ag cathode.

compared. Accordingly, the optimum oleamide doping ratio was determined to be 5 wt % (see SI Figure S1 and Table S1). An overdoping of oleamide in PCBM (>10 wt %) or replacing PCBM ETL by oleamide led to a dramatic decrease of PCE (not shown). Under the optimum oleamide doping ratio of 5 wt %, the current density−voltage (J−V) curve of the oleamide:PCBM ETL-based ISPSC device is shown in Figure 2, which also includes that based on pure PCBM ETL for comparison. The measured photovoltaic parameters (short-circuit current (J_{sc}), open-circuit voltage (V_{oc}), FF, and PCE) are summarized in Table 1.

The reference device based on a pure PCBM ETL shows a V_{oc} of 0.95 V, a J_{sc} of 17.08 mA cm^{-2}, an FF of 61.8%, and a PCE of 10.05%, which is comparable to the reported values with ISPSC devices fabricated under similar conditions.[27−29]

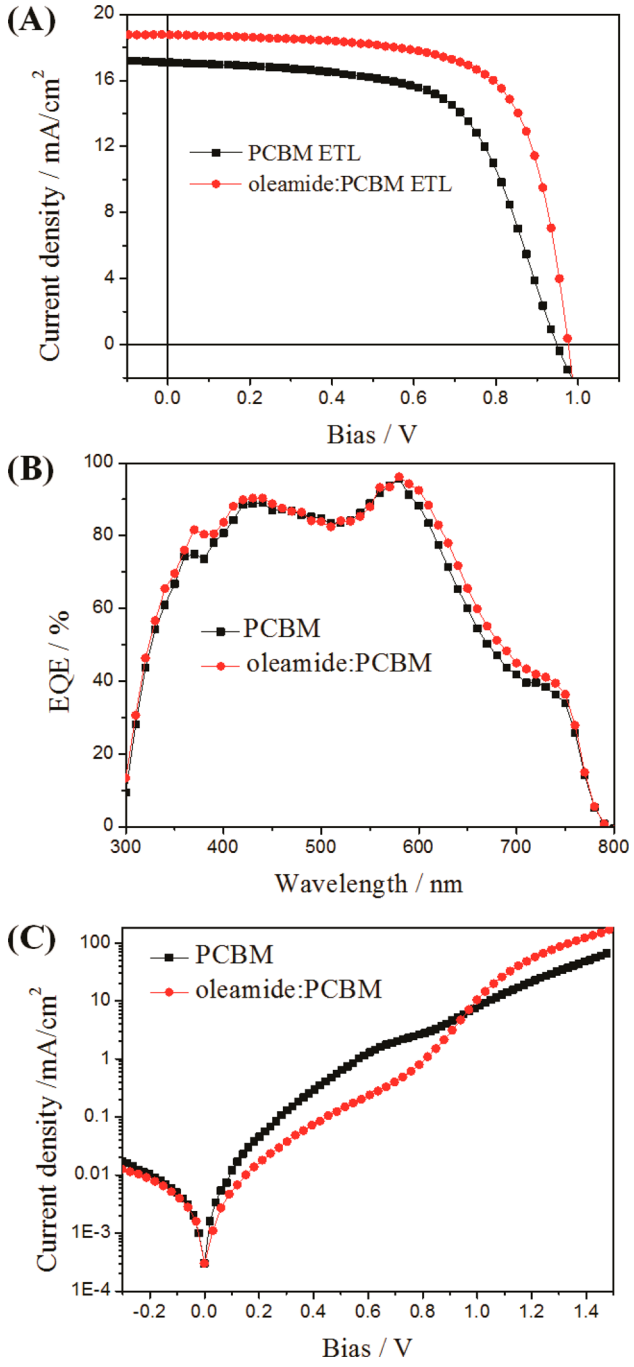

Figure 2. (A) J−V curves of $CH_3NH_3PbI_xCl_{3-x}$ ISPSC devices with pure PCBM or oleamide:PCBM ETL measured under illumination of an AM 1.5 solar simulator (100 mW cm^{-2}) in air. (B) EQE spectra of the devices with or without oleamide measured in air. (C) Logarithmic plot of J−V characteristics of the devices in the dark.

Upon oleamide doping, the PCE increases dramatically to 12.69%, calculated from a V_{oc} of 0.98 V, a J_{sc} of 18.76 mA/cm^2, and an FF of 69.3%. The PCE enhancement of ∼26% relative to that of the reference device is primarily due to the increases of both FF (from 61.8% to 69.3%, ∼12% enhancement) and J_{sc} (from 17.08 to 18.76 mA/cm^2, ∼10% enhancement), while V_{oc} exhibits only a slight increase. We also checked the device performance statistics (PCE, FF, and J_{sc}) for devices with and without oleamide doping. According to our histograms, the average PCE of the reference devices is 8.5%, which increases

DOI: 10.1021/acsami.5b03525
ACS Appl. Mater. Interfaces 2015, 7, 13659−13665

Table 1. Photovoltaic Parameters of the Best ITO/PEDOT:PSS/$CH_3NH_3PbI_xCl_{3-x}$/ETL/Ag ISPSC Devices with Different ETLs Obtained from *J*−*V* Curves under Reverse Scan

ETL	V_{oc} (V)	J_{sc} (mA/cm^2)	FF (%)	PCE (%)	R_s[b] (Ω·cm^2)	R_{sh}[b] (Ω·cm^2)
PCBM	0.95	17.08	61.8	10.05	17.7	961.4
Oleamide:PCBM[a]	0.98	18.76	69.3	12.69	4.8	940.8

[a]Doping ratio of oleamide is 5 wt %. [b]R_s and R_{sh} are given by the PCE measurement system.

to 10.5% for the oleamide:PCBM ETL-based devices. The average FF and J_{sc} increase from 55% to 65% and from 16.5 to 17.5 mA/cm^2, respectively (see SI Figure S2). Besides, the hysteresis of the *J*−*V* curve was also checked for the devices with and without oleamide, indicating that there was a small hysteresis of the *J*−*V* curve for both reference (undoped) and oleamide-doped devices, while the hysteresis for an oleamide-doped device is much smaller than that for the reference (undoped) device (see SI Figure S3 and Table S2). This is probably because the improved surface coverage of the PCBM on the perovskite film upon oleamide doping as discussed below may passivate the grain boundary of perovskite layer.

The external quantum efficiency (EQE) curves of pure PCBM and oleamide:PCBM ETL-based devices are compared in Figure 2B. For both curves, there is a broad band with an EQE of 70−90% in the region of 350−650 nm, which is much lower in the region of 650−800 nm. The EQE response onset at around 800 nm is consistent with the absorption onset as shown in Figure 3. The overall EQE values and integreated

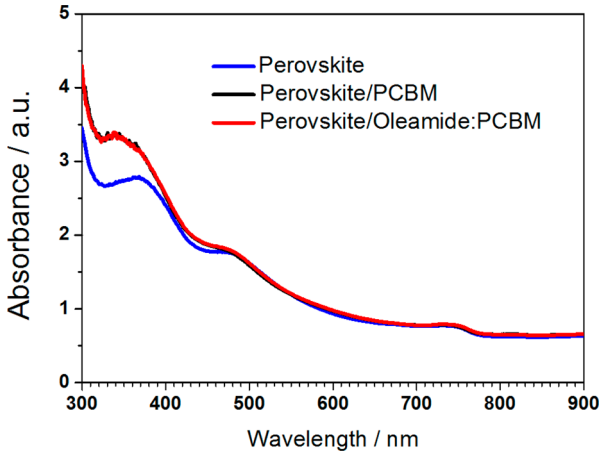

Figure 3. UV−vis absorption spectra of perovskite, perovskite/PCBM, and perovskite/oleamide:PCBM films.

photocurrents of the oleamide:PCBM ETL-based device are larger than those of the pure PCBM ETL-based one, and this is in line with the increase of J_{sc} for oleamide-doped devices, suggesting more efficient electron extraction by the Ag cathode upon oleamide doping.

Since FF is another important photovoltaic parameter responsible for the efficiency enhancement, the factors determining FF are then analyzed. Unlike V_{oc} and J_{sc}, FF is more sensitive to the photoactive layer/electrode interface and is directly correlated with the series resistance (R_s) and shunt resistance (R_{sh}), which can be directly extracted from the *J*−*V* curve.[2,6−12] Upon oleamide doping of PCBM ETL, R_s decreases significantly (from 17.7 to 4.8 Ω·cm^2) while R_{sh} exhibits a slight decrease (see Table 1), suggesting an improved perovskite photoactive layer/cathode interface more favorable for electron transport. In addition, the *J*−*V* curve in the dark provides valuable information on the inherent electrical characteristics, such as R_s, R_{sh}, and the leakage current of the solar cell devices.[27−32] As clearly shown in Figure 2C, the dark current density of the ISPSC devices based on oleamide:PCBM ETL under the reverse bias is lower than that of devices based on pure PCBM ETL, suggesting that the leakage current at the PCBM ETL/cathode is reduced upon oleamide doping.[29] However, in the forward bias region of 0.95−1.5 V, the injected current density of the device with oleamide is much higher than that of the device without oleamide, suggesting a lowered injection barrier between the PCBM ETL and the Ag cathode upon oleamide doping and consequently improved electron transport.[27−29,31,32] Therefore, the decrease of R_s due to the reduced leakage current and improved electron transport is confirmed, accounting for the increase of FF.

Figure 3 compares the UV−vis absorption spectrum of the $CH_3NH_3PbI_xCl_{3-x}$ perovskite/oleamide:PCBM bilayer film with those of perovskite/PCBM and perovskite films for comparison. The absorption onset of the $CH_3NH_3PbI_xCl_{3-x}$ perovskite layer is about 780 nm, which corresponds to an optical bandgap of 1.59 eV. This value is comparable to those reported in the literature for the $CH_3NH_3PbI_xCl_{3-x}$ perovskite film prepared by one-step spin-coating method, which shows good crystallinity as confirmed by XRD characterization (see SI Figure S4).[28,43] After coating the PCBM layer, the light absorption of perovskite/PCBM bilayer film increases obviously in the region of 300−470 nm due to the absorption of PCBM.[29] In the visible light region (470−800 nm), the light absorption of the perovskite/PCBM bilayer film remains almost the same as that of the pure perovskite film. Upon oleamide doping, the UV−vis absorption spectrum of the perovskite/oleamide:PCBM bilayer film looks identical to that of the perovskite/PCBM film, suggesting that oleamide doping in the PCBM layer barely affects the light absorption of the perovskite/PCBM film. This is understandable since oleamide is a small organic molecule having no absorption in the UV and visible light region. Hence, the contribution of light absorption to the increase of J_{sc} can be ruled out.

The performance of the perovskite solar cell is closely associated with the surface morphology and microstructure of perovskite layer.[21,43,44] In order to investigate the effect of oleamide doping on the surface morphology of the perovskite/PCBM bilayer film and consequently the efficiency enhancement of the ISPSC device, we used scanning electron microscopy (SEM) and atomic force microscopy (AFM) to measure the cross-sectional images and surface morphologies of the perovskite/PCBM bilayer film with and without oleamide doping. The surface topographic SEM image of the $CH_3NH_3PbI_xCl_{3-x}$ perovskite film on ITO/PEDOT:PSS substrate and the cross-sectional SEM image of the device are illustrated in Figure 1, parts B and C, respectively, indicating that the perovskite layer with a thickness of ca. 350 nm is very compact and dense, and oleamide doping hardly affects the thickness of the PCBM layer (ca. 80 nm). The influence of oleamide doping on the surface morphology of the perovskite/

DOI: 10.1021/acsami.5b03525
ACS Appl. Mater. Interfaces 2015, 7, 13659−13665

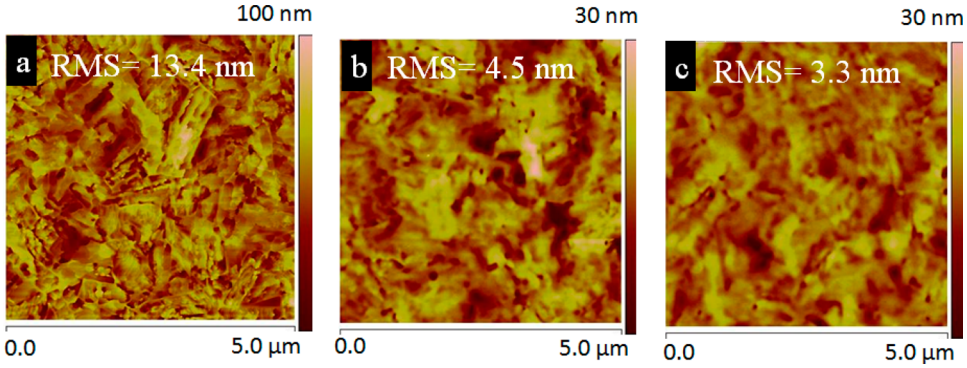

Figure 4. AFM images of the single $CH_3NH_3PbI_xCl_{3-x}$ perovskite film (a), perovskite/PCBM bilayer film (b), and perovskite/oleamide:PCBM bilayer film (c).

PCBM bilayer film is studied by AFM in the tapping mode, as shown in Figure 4a–c (see SI Figure S5 for the section analysis and 3D AFM images). While the 5 μm × 5 μm AFM image of the single perovskite layer shows an inhomogeneous film with a very large root-mean-square (RMS) roughness of 13.4 nm (Figure 4a), that of the perovskite/PCBM bilayer film looks more uniform and smooth, as reflected by the dramatically decreased RMS roughness of 4.5 nm (Figure 4b). Upon oleamide doping in the PCBM layer, although the overall image feature is quite similar to that of the perovskite/PCBM bilayer film, a further decrease in the RMS roughness to 3.3 nm is observed (Figure 4c), indicating that the perovskite/PCBM bilayer film becomes smoother. These results reveal that oleamide doping improves the coverage of the PCBM ETL on the perovskite layer, and a plausible reason is that the intermolecular interaction between the PCBM and the hydrophobic long alkyl chain of the oleamide molecule may prohibit the aggregation of PCBM molecules during solvent evaporation and consequently improve the molecular packing of PCBM. The improved coverage of PCBM ETL on the perovskite layer is beneficial for the interfacial contact between the perovskite layer and the Ag cathode and consequently the electron transport from perovskite to the Ag cathode, as discussed further below.

Impedance spectroscopy is an effective tool to evaluate the interfaces for perovskite solar cells.[45−50] In order to investigate the effect of oleamide doping on the interface between the perovskite layer and the Ag cathode, we measured the impedance spectroscopy of the devices in the dark under a variable reverse potential from 0.2 to 0.8 V.[49,50] The Nyquist plots of the devices with and without oleamide doping under a reverse potential of 0.8 V, which is typically used for perovskite solar cells are compared in Figure 5, which also includes the corresponding fitted curves based on a transmission line model generally used in the literature.[45−50] Accordingly, the data can be well fitted with a simple circuit consisting of a resistor R_s, a charge transfer resistance (R_{rec}), and a constant phase element (CPE) for the interface between the perovskite layer and the Ag cathode (see SI Figure S6). While R_{rec} is dependent on the charge transport process at the interface, CPE, as a nonideal capacitor, is usually defined by CPE-T and CPE-P, which are related to the interface capacitor and an ideal capacitor, respectively. The fitted parameters of R_s, R_{rec}, CPE-T, and CPE-P from Nyquist plots are summarized in Table 2.

Comparing the fitted value of R_S, which is correlated to the internal resistance, we found that the R_S for the device with oleamide (7.15 Ω·cm^2) is smaller than that of the device without oleamide (8.99 Ω·cm^2). This result is consistent with the decrease of the series resistance upon oleamide doping determined from $J-V$ curve, as discussed above. Besides, the fitted value of R_{rec}, which is inversely proportional to charge recombination,[47−49] is 1170 Ω·cm^2 for the device with oleamide, much larger than that of the device without oleamide (611.9 Ω·cm^2) (see also SI Figure S6 for the comparison of R_{rec} under other biases). This suggests that oleamide doping improves the interfacial contact between perovskite layer and Ag cathode, thus prohibiting electron−hole recombination and improving electron transport, and these may result in the loss of electron.[46] This result is consistent with the drastically decreased series resistance (from 17.7 to 4.8 Ω·cm^2) for the oleamide-doped device observed from $J-V$ curve, which mainly reflects the information on charge transport between interfaces. Furthermore, the CPE-T value for the device with oleamide is 5.39 × 10^{-8} F/cm^2, much larger than that for the device without oleamide (1.02 × 10^{-8} F/cm^2). This suggests that the interface capacitance for the device with oleamide is more ideal

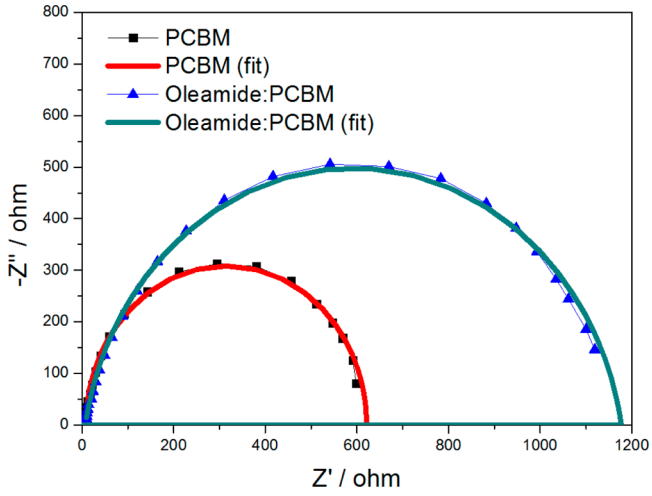

Figure 5. Nyquist plots of the $CH_3NH_3PbI_xCl_{3-x}$ perovskite-based ISPSC devices with and without oleamide in the dark.

Table 2. Parameters Employed for the Fitting of the Impedance Spectra of the Best $CH_3NH_3PbI_xCl_{3-x}$ Perovskite-Based ISPSC Devices with and without Oleamide

ETL	R_S (Ω·cm^2)	R_{rec} (Ω·cm^2)	CPE-T (F/cm^2)	CPE-P
PCBM	8.99	611.9	1.02 × 10^{-8}	1.005
oleamide:PCBM	7.15	1170	5.39 × 10^{-8}	0.898

DOI: 10.1021/acsami.5b03525
ACS Appl. Mater. Interfaces 2015, 7, 13659−13665

electrically than that for the device without oleamide (see Table 2). Consequently, a dramatically enhanced electron collection efficiency for the device with oleamide is expected, and this directly contributes to the increases of both FF and J_{sc}.

CONCLUSIONS

In summary, an amphiphilic surfactant oleamide was introduced into ISPSC for the first time by doping it in PCBM ETL, leading to a dramatic efficiency enhancement of the $CH_3NH_3PbI_xCl_{3-x}$ perovskite-based ISPSC devices. Under the optimized oleamide doping ratio of 5 wt %, PCE of the ISPSC devices increases from 10.05% to 12.69%, and this is primarily due to the increases of both FF and J_{sc}. According to the surface morphology study of the perovskite/PCBM bilayer film, oleamide doping improves the coverage of PCBM ETL onto the perovskite layer, and this is beneficial for the interfacial contact between the perovskite layer and the Ag cathode, and consequently the electron transport from perovskite to the Ag cathode. Impedance spectroscopic study reveals the prohibited electron−hole recombination at the interface between the perovskite layer and the Ag cathode, resulting in dramatically enhanced electron collection efficiency. Our technique of incorporating the surfactant into ETL is simple and effective, providing a new avenue for achieving high efficiency perovskite solar cells.

ASSOCIATED CONTENT

Supporting Information

Performance of ISPSC devices with different oleamide doping ratios, Histograms of PCE, FF and J_{sc}, Hysteresis of $J-V$ curves of the best devices, XRD pattern of $CH_3NH_3PbI_xCl_{3-x}$ perovskite film, section analysis and 3D AFM images, impedance spectra under different biases, and so forth. The Supporting Information is available free of charge on the ACS Publications website at DOI: 10.1021/acsami.5b03525.

AUTHOR INFORMATION

Corresponding Author

*E-mail: sfyang@ustc.edu.cn.

Notes

The authors declare no competing financial interest.

ACKNOWLEDGMENTS

This work was partially supported by National Natural Science Foundation of China (Nos. 21132007, 21371164), Key Project of Hefei Centre for Physical Science and Technology (No. 2012FXZY006), and the Fundamental Research Funds for the Central Universities (WK3430000002).

REFERENCES

(1) Kojima, A.; Teshima, K.; Shirai, Y.; Miyasaka, T. Organometal Halide Perovskites as Visible-Light Sensitizers for Photovoltaic Cells. *J. Am. Chem. Soc.* **2009**, *131*, 6050−6051.

(2) Snaith, H. J. Perovskites: The Emergence of a New Era for Low-Cost, High-Efficiency Solar Cells. *J. Phys. Chem. Lett.* **2013**, *4*, 3623−3630.

(3) Lee, M. M.; Teuscher, J.; Miyasaka, T.; Murakami, T. N.; Snaith, H. J. Efficient Hybrid Solar Cells Based on *meso*-Superstructured Organometal Halide Perovskites. *Science* **2012**, *338*, 643−647.

(4) Xing, G. C.; Mathews, N.; Sun, S. Y.; Lim, S. S.; Lam, Y. M.; Grätzel, M.; Mhaisalkar, S.; Sum, T. C. Long-Range Balanced Electron and Hole Transport Lengths in Organic-Inorganic $CH_3NH_3PbI_3$. *Science* **2013**, *342*, 344−347.

(5) Stranks, S. D.; Eperon, G. E.; Grancini, G.; Menelaou, C.; Alcocer, M. J. P.; Leijtens, T.; Herz, L.; Petrozza, A.; Snaith, H. J. Electron-Hole Diffusion Lengths Exceeding 1 Micrometer in an Organometal Trihalide Perovskite Absorber. *Science* **2013**, *342*, 341−344.

(6) Kim, H. S.; Lee, C. R.; Im, J. H.; Lee, K. B.; Moehl, T.; Marchioro, A.; Moon, S. J.; Humphry-Baker, R.; Yum, J. H.; Moser, J. E.; Grätzel, M.; Park, N. G. Lead Iodide Perovskite Sensitized All-Solid-State Submicron Thin Film Mesoscopic Solar Cell with Efficiency Exceeding 9%. *Sci. Rep.* **2012**, *2*, 591−597.

(7) Heo, J. H.; Im, S. H.; Noh, J. H.; Mandal, T. N.; Lim, C. S.; Chang, J. A.; Lee, Y. H.; Kim, H. J.; Sarkar, A.; Nazeeruddin, M. K.; Grätzel, M.; Seok, S. I. Efficient Inorganic−Organic Hybrid Heterojunction Solar Cells Containing Perovskite Compound and Polymeric Hole Conductors. *Nat. Photonics* **2013**, *7*, 486−491.

(8) Chen, Q.; Zhou, H.; Hong, Z. R.; Lou, S.; Duan, H.; Wang, H.; Liu, Y.; Li, G.; Yang, Y. Planar Heterojunction Perovskite Solar Cells via Vapor-Assisted Solution Process. *J. Am. Chem. Soc.* **2014**, *136*, 622−625.

(9) Zhou, H. P.; Chen, Q.; Li, G.; Luo, S.; Song, T. B.; Duan, H. S.; Hong, Z. R.; You, J. B.; Liu, Y. S.; Yang, Y. Interface Engineering of Highly Efficient Perovskite Solar Cells. *Science* **2014**, *345*, 542−546.

(10) Jeon, N. J.; Noh, H.; Yang, W. S.; Kim, Y. C.; Ryu, S. C.; Seo, J. W.; Seok, S. I. Compositional Engineering of Perovskite Materials for High-Performance Solar Cells. *Nature* **2015**, *10*, 1038−1042.

(11) Mei, A.; Li, X.; Liu, L.; Ku, Z.; Liu, T.; Rong, Y.; Xu, M.; Hu, M.; Chen, J.; Yang, Y.; Grätzel, M.; Han, H. W. A Hole-Conductor-Free, Fully Printable Mesoscopic Perovskite Solar Cell with High Stability. *Science* **2014**, *345*, 295−298.

(12) He, M.; Zheng, D. J.; Wang, M. Y.; Lin, C. J.; Lin, Z. Q. High Efficiency Perovskite Solar Cells: From Complex Nanostructure to Planar Heterojunction. *J. Mater. Chem. A* **2014**, *2*, 5994−6003.

(13) Green, M. A.; Ho-Baillie, A.; Snaith, H. J. The Emergence of Perovskite Solar Cells. *Nat. Photonics* **2014**, *8*, 506−514.

(14) Liu, M.; Johnston, M. B.; Snaith, H. J. Efficient Planar Heterojunction Perovskite Solar Cells by Vapour Deposition. *Nature* **2013**, *501*, 395−398.

(15) Jeon, N. J.; Noh, J. H.; Kim, Y. C.; Yang, W. S.; Ryu, S.; Seok, S. I. Solvent Engineering for High-Performance Inorganic−Organic Hybrid Perovskite Solar Cells. *Nat. Mater.* **2014**, *13*, 897−903.

(16) Lin, Q.; Armin, A.; Nagiri, R. C. R.; Burn, P. L.; Meredith, P. Electro-Optics of Perovskite Solar Cells. *Nat. Photonics* **2014**, *284*, 1038−1044.

(17) Malinkiewicz, O.; Yella, A.; Lee, Y. H.; Espallargas, G. M.; Grätzel, M.; Nazeeruddin, M. K.; Bolink, H. J. Perovskite Solar Cells Employing Organic Charge-Transport Layers. *Nat. Photonics* **2014**, *8*, 128−132.

(18) Jeng, J.; Chiang, Y.; Lee, M.; Peng, S.; Guo, T.; Chen, P.; Wen, T. $CH_3NH_3PbI_3$ Perovskite/Fullerene Planar−Heterojunction Hybrid Solar Cells. *Adv. Mater.* **2013**, *25*, 3727−3732.

(19) You, J.; Hong, Z.; Yang, Y. M.; Chen, Q.; Cai, M.; Song, T. B.; Chen, C. C.; Lu, S.; Liu, Y.; Zhou, H.; Yang, Y. Low-Temperature Solution-Processed Perovskite Solar Cells with High Efficiency and Flexibility. *ACS Nano* **2014**, *8*, 1674−1680.

(20) Sun, S.; Salim, T.; Mathews, N.; Duchamp, M.; Boothroyd, C.; Xing, G.; Sum, T. C.; Lam, Y. M. The Origin of High Efficiency in Low-Temperature Solution-Processable Bilayer Organometal Halide Hybrid Solar Cells. *Energy Environ. Sci.* **2014**, *7*, 399−407.

(21) Xiao, Z.; Dong, Q.; Bi, C.; Shao, Y.; Yuan, Y.; Huang, J. S. Solvent Annealing of Perovskite-Induced Crystal Growth for Photovoltaic-Device Efficiency Enhancement. *Adv. Mater.* **2014**, *26*, 6503−6509.

(22) Seo, J.; Park, S.; Kim, Y. C.; Jeon, N. J.; Noh, J. H.; Yoon, S. C.; Seok, S. I. Benefits of Very Thin PCBM and LiF Layers for Solution-Processed *p-i-n* Perovskite Solar Cells. *Energy Environ. Sci.* **2014**, *7*, 2642−2646.

(23) Wang, Q.; Shao, Y.; Dong, Q.; Xiao, Z.; Yuan, Y.; Huang, J. S. Large Fill-Factor Bilayer Iodine Perovskite Solar Cells Fabricated by a

DOI: 10.1021/acsami.5b03525
ACS Appl. Mater. Interfaces 2015, 7, 13659−13665

Low-Temperature Solution-Process. *Energy Environ. Sci.* **2014**, *7*, 2359−2365.
(24) Docampo, P.; Ball, J. M.; Darwich, M.; Eperon, G. E.; Snaith, H. J. Efficient Organometal Trihalide Perovskite Planar−Heterojunction Solar Cells on Flexible Polymer Substrates. *Nat. Commun.* **2013**, *4*, 2761−2766.
(25) Nie, W.; Tsai, H.; Asadpour, R.; Blancon, J. C.; Neukirch, A. J.; Gupta, G.; Crochet, J. J.; Chhowalla, M.; Tretiak, S.; Alam, M. A.; Wang, H. L.; Mohite, A. D. High-Efficiency Solution-Processed Perovskite Solar Cells with Millimeter-Scale Grains. *Science* **2015**, *347*, 522−525.
(26) Li, G.; Zhu, R.; Yang, Y. Polymer Solar Cells. *Nat. Photonics* **2012**, *6*, 153−161.
(27) Chen, Y. H.; Chen, T.; Dai, L. M. Layer-by-Layer Growth of $CH_3NH_3PbI_{3-x}Cl_x$ for Highly Efficient Planar Heterojunction Perovskite Solar Cells. *Adv. Mater.* **2015**, *27*, 1053−1059.
(28) Liu, X.; Yu, H.; Yan, L.; Dong, Q.; Wan, Q.; Zhou, Y.; Song, B.; Li, Y. F. Triple Cathode Buffer Layers Composed of PCBM, C60, and LiF for High-Performance Planar Perovskite Solar Cells. *ACS Appl. Mater. Interfaces* **2015**, *7*, 6230−6237.
(29) Xue, Q.; Hu, Z.; Liu, J.; Lin, J.; Sun, C.; Chen, Z.; Duan, C.; Wang, J.; Liao, C.; Lau, W. M.; Huang, F.; Yip, H. L.; Cao, Y. Highly Efficient Fullerene/Perovskite Planar Heterojunction Solar Cells via Cathode Modification with an Amino-Functionalized Polymer Interlayer. *J. Mater. Chem. A* **2014**, *2*, 19598−19603.
(30) You, J.; Yang, Y.; Hong, Z.; Song, T. B.; Meng, L.; Liu, Y.; Jiang, C.; Zhou, H.; Chang, W. H.; Li, G.; Yang, Y. Moisture Assisted Perovskite Film Growth for High Performance Solar Cells. *Appl. Phys. Lett.* **2014**, *105*, 183902−183905.
(31) Liang, P. W.; Liao, C. Y.; Chueh, C. C.; Zuo, F.; Williams, S. T.; Xin, X. K.; Lin, J.; Jen, A. K. Y. Additive Enhanced Crystallization of Solution-Processed Perovskite for Highly Efficient Planar−Heterojunction Solar Cells. *Adv. Mater.* **2014**, *26*, 3748−3754.
(32) Min, J.; Zhang, Z. G.; Hou, Y.; Quiroz, C. O. R.; Przybilla, T.; Bronnbauer, C.; Guo, F.; Forberich, K.; Azimi, H.; Ameri, T.; Spiecker, E.; Li, Y. F.; Brabec, C. J. Interface Engineering of Perovskite Hybrid Solar Cells with Solution-Processed Perylene−Diimide Heterojunctions toward High Performance. *Chem. Mater.* **2015**, *27*, 227−234.
(33) Bai, Y.; Yu, H.; Zhu, Z.; Jiang, K.; Zhang, T.; Zhao, N.; Yang, S. H.; Yan, H. High Performance Inverted Structure Perovskite Solar Cells Based on a PCBM:Polystyrene Blend Electron Transport Layer. *J. Mater. Chem. A* **2015**, *10*, 1039−1043.
(34) Etgar, L.; Gao, P.; Xue, Z.; Peng, Q.; Chandiran, A. K.; Liu, B.; Nazeeruddin, M. K.; Grätzel, M. Mesoscopic $CH_3NH_3PbI_3/TiO_2$ Heterojunction Solar Cells. *J. Am. Chem. Soc.* **2012**, *134*, 17396−17399.
(35) Heeger, A. J. 25th Anniversary Article: Bulk Heterojunction Solar Cells: Understanding the Mechanism of Operation. *Adv. Mater.* **2014**, *26*, 10−28.
(36) He, Z. C.; Wu, H. B.; Cao, Y. Recent Advances in Polymer Solar Cells: Realization of High Device Performance by Incorporating Water/Alcohol-Soluble Conjugated Polymers as Electrode Buffer Layer. *Adv. Mater.* **2014**, *26*, 1006−1024.
(37) Yip, H. L.; Jen, A. K. Y. Recent Advances in Solution-Processed Interfacial Materials for Efficient and Stable Polymer Solar Cells. *Energy Environ. Sci.* **2012**, *5*, 5994−6011.
(38) Page, Z. A.; Liu, Y.; Duzhko, V. V.; Russell, T. P.; Emrick, T. Fulleropyrrolidine Interlayers: Tailoring Electrodes to Raise Organic Solar Cell Efficiency. *Science* **2014**, *346*, 441−444.
(39) Wang, H. T.; Zhang, W. F.; Xu, C. H.; Bi, X. H.; Chen, B. X.; Yang, S. F. Efficiency Enhancement of Polymer Solar Cells by Applying Poly(vinylpyrrolidone) as a Cathode Buffer Layer via Spin Coating or Self-Assembly. *ACS Appl. Mater. Interfaces* **2013**, *5*, 26−34.
(40) Qu, S. X.; Li, M. H.; Xie, L. X.; Huang, X.; Yang, J. G.; Wang, N.; Yang, S. F. Noncovalent Functionalization of Graphene Attaching [6,6]-Phenyl-C61-Butyric Acid Methyl Ester (PCBM) and Application as Electron Extraction Layer of Polymer Solar Cells. *ACS Nano* **2013**, *7*, 4070−4081.
(41) Zhao, X. M.; Xu, C. H.; Wang, H. T.; Chen, F.; Zhang, W. F.; Zhao, Z. Q.; Chen, L. W.; Yang, S. F. Application of Biuret, Dicyandiamide, or Urea as a Cathode Buffer Layer toward the Efficiency Enhancement of Polymer Solar Cells. *ACS Appl. Mater. Interfaces* **2014**, *6*, 4329−4337.
(42) Zhang, W. F.; Wang, H. T.; Chen, B. X.; Bi, X. H.; Venkatesan, S.; Qiao, Q. Q.; Yang, S. F. Oleamide as a Self-Assembled Cathode Buffer Layer for Polymer Solar Cells: The Role of the Terminal Group on the Function of the Surfactant. *J. Mater. Chem.* **2012**, *22*, 24067−24074.
(43) Xiao, M.; Huang, F.; Huang, W.; Dkhissi, Y.; Zhu, Y.; Etheridge, J.; Gray-Weale, A.; Bach, U.; Cheng, Y. B.; Spiccia, L. A Fast Deposition-Crystallization Procedure for Highly Efficient Lead Iodide Perovskite Thin-Film Solar Cells. *Angew. Chem., Int. Ed.* **2014**, *53*, 9898−9903.
(44) Eperon, G. E.; Burlakov, V. M.; Docampo, P.; Goriely, A.; Snaith, H. J. Morphological Control for High Performance, Solution-Processed Planar Heterojunction Perovskite Solar Cells. *Adv. Funct. Mater.* **2014**, *24*, 151−157.
(45) Kim, H. S.; Mora-Sero, I.; Gonzalez-Pedro, V.; Fabregat-Santiago, F.; Juarez-Perez, E. J.; Park, N. G.; Bisquert, J. Mechanism of Carrier Accumulation in Perovskite Thin-Absorber Solar Cells. *Nat. Commun.* **2013**, *4*, 2242−2248.
(46) Dualeh, A.; Moehl, T.; Tétreault, N.; Teuscher, J.; Gao, P.; Nazeeruddin, M. K.; Grätzel, M. Impedance Spectroscopic Analysis of Lead Iodide Perovskite-Sensitized Solid-State Solar Cells. *ACS Nano* **2014**, *8*, 362−373.
(47) Gonzalez-Pedro, V.; Juarez-Perez, E. J.; Arsyad, W. S.; Barea, E. M.; Fabregat-Santiago, F.; Mora-Sero, I.; Bisquert, J. General Working Principles of $CH_3NH_3PbX_3$ Perovskite Solar Cells. *Nano Lett.* **2014**, *14*, 888−893.
(48) Juarez-Perez, E. J.; Wußler, M.; Fabregat-Santiago, F.; Lakus-Wollny, K.; Mankel, E.; Mayer, T.; Jaegermann, W.; Mora-Sero, I. Role of the Selective Contacts in the Performance of Lead Halide Perovskite Solar Cells. *J. Phys. Chem. Lett.* **2014**, *5*, 680−685.
(49) Pockett, A.; Eperon, G. E.; Peltola, T.; Snaith, H. J.; Walker, A.; Peter, L. M.; Cameron, P. J. Characterization of Planar Lead Halide Perovskite Solar Cells by Impedance Spectroscopy, Open-Circuit Photovoltage Decay, and Intensity-Modulated Photovoltage/Photocurrent Spectroscopy. *J. Phys. Chem. C* **2015**, *119*, 3456−3465.
(50) Wang, W. W.; Yuan, J. Y.; Shi, G. Z.; Zhu, X. X.; Shi, S. H.; Liu, Z. K.; Han, L.; Wang, H. Q.; Ma, W. L. Inverted Planar Heterojunction Perovskite Solar Cells Employing Polymer as the Electron Conductor. *ACS Appl. Mater. Interfaces* **2015**, *7*, 3994−3999.

DOI: 10.1021/acsami.5b03525
ACS Appl. Mater. Interfaces 2015, 7, 13659−13665